Predictive Torque Control Scheme for Three-Phase Four-Switch Inverter-Fed Induction Motor Drives With DC-Link Voltages Offset Suppression

Dehong Zhou, Jin Zhao, *Member, IEEE*, and Yang Liu, *Member, IEEE*

***Abstract*—The four-switch three-phase (B4) inverter, having a lower number of switches, was first presented for the possibility of reducing the inverter cost, and it became very attractive as it can be utilized in fault-tolerant control to solve the open/short-circuit fault of the six-switch three-phase (B6) inverter. However, the balance among the phase currents collapses due to the fluctuation of the two dc-link capacitor voltages; therefore, its application is limited. This paper proposes a predictive torque control (PTC) scheme for the B4 inverter-fed induction motor (IM) with the dc-link voltage offset suppression. The voltage vectors of the B4 inverter under the fluctuation of the two dc-link capacitor voltages are derived for precise prediction and control of the torque and stator flux. The three-phase currents are forced to stay balance by directly controlling the stator flux. The voltage offset of the two dc-link capacitors is modeled and controlled in the predictive point of view. A lot of simulation and experimental results are presented to validate the proposed control scheme.**

***Index Terms*—Cost function, current unbalance, four-switch inverter, induction motor (IM) drives, model predictive control (MPC).**

I. Introduction

OVER the years, the conventional three-phase voltage-source inverter with six switches (B6) has been found widespread industrial applications in various forms, such as motor drives and active filters. However, in certain applications, a further cost reduction for inverter configuration is considered by users. To achieve this goal, the three-phase inverter with only four switches was proposed by Van der Broeck and Van Wyk [1] for the purpose of minimizing the components' cost, and it is named four-switch three-phase (B4) inverter in comparison with the B6 one, as shown in Fig. 1. Although this kind of cost reduction is at the expense of output performance, the B4 inverter can be utilized in fault-tolerant control to solve the open/short-circuit fault of the B6 inverter. The idea of the B4 inverter applied to fault-tolerant control is very valuable in some critical occasions such as rail traction, and it has consequently attracted the interest of many researchers [2]–[11].

Manuscript received April 7, 2014; revised June 1, 2014 and July 1, 2014; accepted July 6, 2014. Date of publication July 14, 2014; date of current version January 16, 2015. This work was supported by the National Natural Science Foundation of China under Grant 61273174 and Grant 61034006. Recommended for publication by Associate Editor R. Kennel.

The authors are with the Key Laboratory of Image Information Processing and Intelligent Control, Ministry of Education, and the School of Automation, Huazhong University of Science and Technology, Hubei 430074, China (e-mail: zhoudehong@hust.edu.cn; jinzhao617@163.com; Yangliu30@gmail.com).

Color versions of one or more of the figures in this paper are available online at http://ieeexplore.ieee.org.

Digital Object Identifier 10.1109/TPEL.2014.2338395

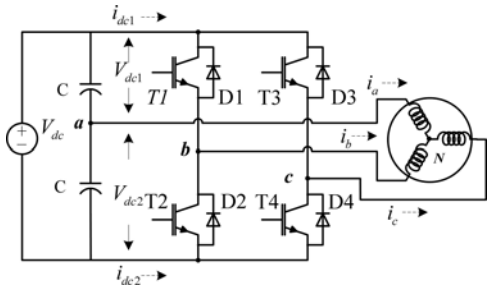

Fig. 1. Circuit diagrams of a B4 inverter-fed induction motor drive.

The four-switch inverters are known to have several disadvantages compared to normal six-switch inverters: the voltage utilization factor is halved compared to the six-switch inverter. On the other hand, the capacitor center tap voltage is fluctuating, and it destroys the balance among the motor phase currents [12]. The capacitor center tap voltage fluctuation increases as the load torque becomes higher or the frequency of a B4 inverter becomes lower, and the unbalanced motor current leads to an inverter failure and torque pulsation [13].

In order to mitigate the effects of the capacitor center tap voltage fluctuation, several papers were published. An adaptive space vector modulation (SVM) approach was proposed to compensate the dc-link voltage ripple in a B4 inverter [12]. Kim *et al*. [13] investigated motor current unbalance from the perspective of source impedance and the voltage variation caused by the current flowing through the capacitor, and proposed a current distortion compensation scheme. Lee *et al*. [14] proposed a compensation method by adjusting switching times considering the capacitor center tap voltage fluctuation. Wang *et al*. [15] investigated the cause and effect of the capacitor center tap voltage fluctuation in analytical point of view, and the capacitor voltage offset was suppressed by employing certain switching states. However, the capacitor voltage offset suppression was achieved at the expense of the B4 inverter's output performance. The works mentioned earlier were dedicated to obtain the balanced three-phase currents of the B4 inverter, but the flux and torque control was not considered.

Regarding the flux and torque control of a B4 inverter-fed IM drive, several papers on closed-loop control scheme were published. Uddin *et al*. [16] discussed a closed-loop vector control scheme for a B4 inverter-fed IPM synchronous motor, in which the current loop was controlled by a hysteresis controller and the speed loop was controlled by a fuzzy-logic controller.

Kashif *et al*. [17] utilized a three-layer feed-forward back propagation artificial neural network for flux control of a B4 inverter-fed IM drive. El Badsi *et al*. [18] used a DTC scheme for torque and flux control of a B4 inverter-fed IM drive. Unfortunately, the two capacitor voltages were assumed constant in these papers. In fact, as a result of one-phase current flows through the split dc-link voltage sources, the fluctuation will inevitably appear in the two capacitor voltages, which deteriorates the output performance of the B4 inverter (i.e., torque pulsation and unbalanced three-phase currents). More seriously, if the balanced condition of the currents flowing in the two capacitor voltages is corrupted, the two capacitor voltages will deviate in two opposite directions till shutting down of the B4 inverter.

With the development of fast and powerful microprocessors, increasing attention has been dedicated to the use of model predictive control (MPC) in power electronics [19]. The first ideas about this strategy applied to power converters started in the 1980s [20], [21]. The main concept is based on calculating the system's future behavior to obtain optimal values for the actuating variables. With this intuitive concept, predictive control can be applied to a variety of systems, in which constraints and nonlinearities can be easily included, multivariable case can be considered, and the resulting controller is easy to implement [22]. These features render the approach very attractive and effective for the control of power electronics system [23], [24], including drive control [25]–[27], especially predictive torque control (PTC; particular for a two-level converter with horizon $N = 1$).

In the PTC, the complete model and future behavior of the inverter-fed drives are taken into account. A cost function relating to torque and flux errors reduction is defined to evaluate the effects of each voltage vector and the one minimizing the cost function is selected [28]–[36]. In spite of the outstanding performance of B6 inverter-fed drives based on the PTC, PTC for B4 inverter-fed drives did not get many attentions to the researchers. Some simulation results of PTC for the B4 inverter-fed drives emulating the B6 case were carried out in [36]. However, the dc-link voltages fluctuation, which is the intrinsic feature of the B4 inverter, was not considered. Additionally, and the offset suppression of the two capacitor voltages was not mentioned.

In this paper, the special issues on using the famous PTC control scheme for B4 inverter-fed IM drives are analyzed and discussed. Each half dc-link voltage is measured to achieve precise prediction and control of torque and stator flux. The voltage vectors of the B4 inverter under the fluctuation of the two dc-link capacitor voltages are derived for precise prediction and control of the torque and stator flux. The closed-loop control of torque and stator flux is achieved by the cost function in the PTC. The balanced three-phase currents are achieved by controlling the stator flux well. The capacitor voltage offset is modeled and suppressed in the predictive point of view. The effectiveness of the proposed scheme is demonstrated by extensive simulation and experimental results. Because of the halved switch states corresponding to B6 one, the real-time implementation time cost for the PTC scheme in B4 inverter is reduced in a sampling period. This paper is organized as follows. In Section II, the model of B4 inverter and induction motor (IM) is illustrated.

TABLE I
SWITCHING FUNCTION AND THE OUTPUT VOLTAGES OF THE B4 INVERTER

States		Switch On		Output Voltage		
S_b	S_c			V_{aN}	V_{bN}	V_{cN}
0	0	T2	T4	$2 \cdot V_{\mathrm{dc}2/3}$	$-V_{\mathrm{dc}2}/3$	$-V_{\mathrm{dc}2}/3$
0	1	T2	T3	$(V_{\mathrm{dc}2}-V_{\mathrm{dc}1})/3$	$-(2V_{\mathrm{dc}2}+V_{\mathrm{dc}1})/3$	$(2V_{\mathrm{dc}1}+V_{\mathrm{dc}2})/3$
1	0	T1	T4	$(V_{\mathrm{dc}2}-V_{\mathrm{dc}1})/3$	$(2V_{\mathrm{dc}1}+V_{\mathrm{dc}2})/3$	$-(2V_{\mathrm{dc}2}+V_{\mathrm{dc}1})/3$
1	1	T1	T3	$-2V_{\mathrm{dc}1}/3$	$V_{\mathrm{dc}1}/3$	$V_{\mathrm{dc}1}/3$

The proposed PTC control scheme with capacitor voltage suppression is explained in Section III. The weight factors in the cost function are analyzed and discussed in Section IV. In Section V, experimental results are shown. The conclusions are presented in Section VI.

II. MODELING OF THE B4 INVERTER AND IM

A. Intrinsic Voltage Vector of a B4 Inverter

The B4 topology consists of a two-leg inverter, as illustrated in Fig. 1. The dc-link is split into two voltage sources, to the middle of which one load phase is connected. For convenient analysis, the inverter is considered for implementation by ideal switches (T1–T4) (i.e., with no dead time and no saturation voltage drop). This means, the switching states of leg b (T1–T2) and leg c (T3-T4) can be denoted as binary states variables S_b and S_c. To prevent the short circuit of the dc-link, the simultaneous closed states of two switches in each leg are usually forbidden. Therefore, a binary "1" will indicate the close state of the upper switch, whereas a binary "0" will indicate the close state of the lower switch. The basic voltage vectors can be defined according to the switching states.

Assume that the three-phase voltages are balanced, the phase-to-neutral voltages V_{aN},V_{bN},V_{cN} are given as follows:

$$\begin{aligned} V_{aN} &= \tfrac{V_{\mathrm{dc}1}}{3}(-S_b - S_c) + \tfrac{V_{\mathrm{dc}2}}{3}(2 - S_b - S_c) \\ V_{bN} &= \tfrac{V_{\mathrm{dc}1}}{3}(2 \cdot S_b - S_c) + \tfrac{V_{\mathrm{dc}2}}{3}(2 \cdot S_b - S_c - 1) \\ V_{cN} &= \tfrac{V_{\mathrm{dc}1}}{3}(2 \cdot S_c - S_b) + \tfrac{V_{\mathrm{dc}2}}{3}(2 \cdot S_c - S_b - 1) \end{aligned} \quad (1)$$

where $V_{\mathrm{dc}1}$ and $V_{\mathrm{dc}2}$ are the upper and the lower dc-link capacitor voltages, respectively.

Considering all the possible combinations of (S_b, S_c), phase-to-neutral voltages values are given in Table I.

The Clarke transform applied to the stator voltages yields as follows:

$$\begin{bmatrix} V_{\alpha s} \\ V_{\beta s} \end{bmatrix} = \frac{2}{3}\begin{bmatrix} 1 & -\frac{1}{2} & -\frac{1}{2} \\ 0 & \frac{\sqrt{3}}{2} & -\frac{\sqrt{3}}{2} \end{bmatrix}\begin{bmatrix} V_{aN} \\ V_{bN} \\ V_{cN} \end{bmatrix} \quad (2)$$

where the $V_{\alpha s}$ and $V_{\beta s}$ are the α- and β-axis stator voltage, respectively. The voltage vectors are expressed by $\overrightarrow{u_s} = V_\alpha + j^* V_\beta$. Therefore, the four active voltage vectors (V_1 to V_4) in the $\alpha\beta$ plane are given in Table II.

It is clearly revealed that in Table II, the B4 inverter can only produce four basic nonzero voltage vectors. The basic voltage

TABLE II
BASIC VOLTAGE VECTORS OF THE B4 INVERTER

Switching State $(S_b\, S_c)$	Voltage Vector ($\vec{v}_s$)	Vector Symbol
00	$2 \cdot V_{\rm dc2}/3$	V_1
10	$(V_{\rm dc2} - V_{\rm dc1})/3 - j \cdot \sqrt{3}(V_{\rm dc1} + V_{\rm dc2})/3$	V_2
11	$(V_{\rm dc2} - V_{\rm dc1})/3 + j \cdot \sqrt{3}(V_{\rm dc1} + V_{\rm dc2})/3$	V_3
01	$-2 \cdot V_{\rm dc1}/3$	V_4

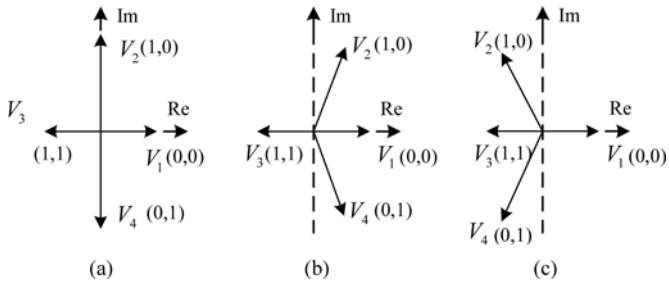

Fig. 2. Basic voltage vectors of the B4 inverter in the case of: (a) $V_{\rm dc1} = V_{\rm dc2}$, (b) $V_{\rm dc1} < V_{\rm dc2}$, and (c) $V_{\rm dc1} > V_{\rm dc2}$.

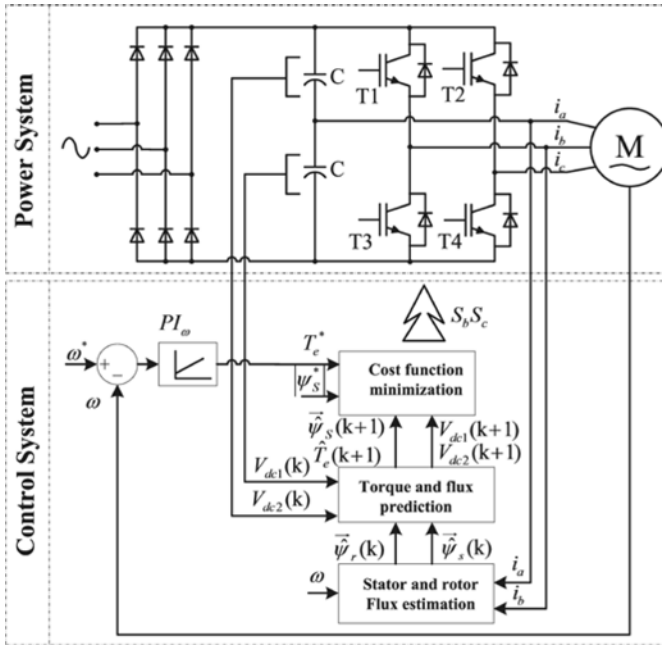

Fig. 3. Structure of the B4 inverter-fed IM drive based on the PTC scheme.

vectors change in amplitude and angle in case of dc-link voltage are not equal. If the values of the upper and lower capacitance are big enough to keep the capacitor voltages a constant value of $V_{\rm dc}/2$, the four voltage vectors produced by the four kinds of switching combination are presented in Fig. 2(a). Otherwise, a ripple in the two capacitor voltages leads to a deviation of these vectors from the previous positions. The vector positions are presented in Fig. 2(b) and (c) in the situation of $V_{\rm dc1} < V_{\rm dc2}$ and $V_{\rm dc1} > V_{\rm dc2}$, respectively. Therefore, the vector positions are calculated as given in Fig. 2.

B. Machine Equations

Stator variables, voltage $\overrightarrow{v_s}$, current $\overrightarrow{i_s}$, and flux $\overrightarrow{\Psi_s}$ are electrically related according to

$$\overrightarrow{v_s} = R_s \overrightarrow{i_s} + \frac{d\overrightarrow{\Psi_s}}{dt} \tag{3}$$

where R_s is the stator resistance.

Rotor equation in a stator reference frame represents the relation between rotor current $\overrightarrow{i_r}$ and rotor flux $\overrightarrow{\Psi_r}$ as follows:

$$0 = R_r \overrightarrow{i_r} + \frac{d\overrightarrow{\Psi_r}}{dt} - j\omega\overrightarrow{\Psi_r} \tag{4}$$

where R_r is the rotor resistance and ω is the rotor speed.

Flux linkage equations relate stator and rotor currents are given in (5) and (6), where L_m, L_s, and L_r are the mutual, stator, and rotor inductances, respectively

$$\overrightarrow{\Psi_s} = L_s \cdot \overrightarrow{i_s} + L_m \cdot \overrightarrow{i_r} \tag{5}$$

$$\overrightarrow{\Psi_r} = L_m \cdot \overrightarrow{i_s} + L_r \cdot \overrightarrow{i_r}. \tag{6}$$

Electromagnetic torque T_e can be expressed in terms of stator current and stator flux

$$T_e = \frac{3}{2} p \overrightarrow{\Psi}_s \times \overrightarrow{i_s} \tag{7}$$

where *p* is the number of pole pairs.

The ratio of change in the mechanical rotor speed ω by the torque

$$J\frac{d\omega}{dt} = T_e - T_L \tag{8}$$

where the coefficient *J* denotes the moment of inertia of the mechanical shaft, and T_L is the load torque to the machine.

III. PROPOSED SCHEME FOR THE B4 INVERTER-FED IM DRIVE

In the proposed scheme, the inner loop is a stator flux and electromagnetic torque controller based on PTC, while the outer speed loop is a traditional PI controller. As in any standard PTC scheme, a three-step algorithm is carried out: flux estimation, flux and torque prediction, and cost function optimization [29], [33]. The structure of the B4 inverter-fed IM drive-based PTC scheme is shown in Fig. 3.

A. Flux Estimation

It is worthwhile to note that the voltage-model-based flux estimator using the command voltages can approximately estimate the stator flux in the B6 case [33]. In a B6 inverter, the dc-link voltage ripple existence means a proportional alteration of all three output phase voltages and accordingly an amplitude error of the average voltage vector used. In a B4 inverter, the voltage ripple leads to different modification of the voltages on the three phase (see Table I) and to both amplitude and angular errors of the switching voltage vectors. Moreover, a significant

fluctuation of the dc-link voltages is inevitable due to one-phase current flows through the split dc-link voltage sources. Hence, the voltage-model-based flux estimator using the command voltages becomes less accurate in the B4 case.

Here, a current-model-based flux estimator using instant currents and speed signals are adopted in the proposed scheme and the estimations of the stator flux $\overrightarrow{\Psi_s}$ and the rotor flux $\overrightarrow{\Psi_r}$ at the present sampling step *k* are required. The rotor flux can be calculated using equivalent equation of an induction machine the rotor dynamics

$$\overrightarrow{\Psi_r} + \tau_r \cdot \frac{d\overrightarrow{\Psi_r}}{dt} = -j\tau_r \cdot (\omega_k - \omega) \cdot \overrightarrow{\Psi_r} + L_m \cdot \overrightarrow{i_s} \quad (9)$$

where $\tau_r = L_r/R_r$, ω_k is the angular speed of a rotating coordinate frame, and ω corresponds to the rotor speed.

Writing (9) in terms of a rotating reference frame aligned with the stator winding ($\omega_k = 0$) is given as follows:

$$\overrightarrow{\Psi_r} + \tau_r \cdot \frac{d\overrightarrow{\Psi_r}}{dt} = L_m \cdot \overrightarrow{i_s} + j\omega \cdot \tau_r \cdot \overrightarrow{\Psi_r}. \quad (10)$$

For the stator flux estimation, the rotor linkage (6) is used to write the rotor current in terms of the measured stator currents and the estimated rotor flux. Then, by replacing $\overrightarrow{i_r}$ of (6) in the stator flux (5), the stator flux estimation is obtained

$$\overrightarrow{\Psi}_s = L_m \cdot \left(\frac{\overrightarrow{\Psi}_r - L_m \cdot \overrightarrow{i_s}}{L_r} \right) + L_r \cdot \overrightarrow{i_r}. \quad (11)$$

Using Euler-based discretization in (10) and(11), the discrete equations of the rotor and stator flux estimation are as follows:

$$\overrightarrow{\hat{\Psi}}_r(k) = \frac{\tau_r}{T_s(1 - j\omega \cdot \tau_r)} \cdot \overrightarrow{\hat{\Psi}}_r(k-1) + \frac{L_m}{1 - j\omega \cdot \tau_r} \cdot \vec{i}_s(k) \quad (12)$$

$$\overrightarrow{\hat{\Psi}}_s(k) = k_r \cdot \overrightarrow{\hat{\Psi}}_r(k) + \sigma L_s \cdot \vec{i}_s(k) \quad (13)$$

where T_s corresponds to the sampling time, $k_r = L_m/L_r$ is the rotor coupling factor and $\sigma = 1 - (L_m^2/L_s L_r)$ is the total leakage factor.

As it is clear to see in (12), the rotor flux estimation is obtained without using the command voltages. Thus, the accurate flux estimation for the B4 inverter-fed IM is achieved.

B. Stator Flux and Electromagnetic Torque Prediction

Since the control variables are stator flux and electromagnetic torque, their behaviors must be predicted at sampling step $k+1$. The stator flux prediction $\overrightarrow{\hat{\Psi}}_s(k+1)$ is obtained by the stator voltage equation. Using the Euler formula to discretize (3) and shifting the result to a single time step, the stator flux prediction is obtained

$$\overrightarrow{\hat{\Psi}}_s(k+1) = \overrightarrow{\hat{\Psi}}_s(k) + T_s \cdot \vec{v}_s(k) - R_s T_s \cdot \vec{i}_s(k) \quad (14)$$

where T_s is the sampling time used in the PTC algorithm. The electromagnetic torque prediction can be calculated as

$$\hat{T}_e(k+1) = \frac{3}{2} p \cdot \mathrm{Im}\left\{ \overrightarrow{\hat{\Psi}}_s(k+1) \cdot \vec{i}_s(k+1) \right\}. \quad (15)$$

The prediction expression of the stator current $\vec{i}_s(k+1)$ is obtained using the equivalent equation of the stator dynamics of an induction machine

$$\vec{v}_s = R_\sigma \cdot \vec{i}_s + L_\sigma \cdot \frac{d\vec{\Psi}_s}{dt} - k_r \cdot \left(\frac{1}{\tau_r} - j \cdot \omega \right) \cdot \vec{\Psi}_r \quad (16)$$

where $R_\sigma = R_s + k_r^2 R_r$ corresponds to the equivalent resistance and $L_\sigma = \sigma L_s$ is the leakage inductance of the machine. The last term in (16) represents the cross coupling between the rotor and the stator winding through the induced voltage. Thus, replacing the derivatives with the Euler formula in (16), the prediction equation of the stator current $\vec{i}_s$ at the instant $k+1$ is obtained

$$\overrightarrow{\hat{i}_s}(k+1) = \left(1 + \frac{T_s}{\tau_\sigma}\right) \cdot \vec{i}_s(k) + \frac{T_s}{\tau_\sigma + T_s} \cdot \left\{ \frac{1}{R_\sigma} \cdot \left(\left(\frac{k_r}{\tau_r} - j \cdot k_r \cdot \omega \right) \cdot \overrightarrow{\hat{\Psi}}_r(k) + \vec{v}_s(k) \right) \right\}. \quad (17)$$

Once the predictions of the stator flux (14) and the stator current (17) are obtained, the prediction of the electromagnetic torque can be calculated in (15).

C. Cost Function Optimization

The next step in predictive control is the optimization of an appropriate control law that is defined as a cost function. The structure form of the cost function is given as follows:

$$\boldsymbol{g}_i = \frac{\left| T_e^* - \hat{T}_e(k+1)_i \right|}{T_{e_{\mathrm{nom}}}} + \lambda_0 \frac{\left| \left\| \vec{\Psi}_s^* \right\| - \left\| \overrightarrow{\hat{\Psi}}_s(k+1)_i \right\| \right|}{\left\| \vec{\Psi}_s \right\|_{\mathrm{nom}}} \quad i \in \{1,2,3,4\} \quad (18)$$

where i denotes the index of the stator voltage vector used to calculate the predictions $\hat{T}_e(k+1)$ and $\overrightarrow{\hat{\Psi}}_s(k+1)$, respectively. The rated torque $T_{e_{\mathrm{nom}}}$ and the rated stator flux magnitude $\left\| \vec{\Psi}_s \right\|_{\mathrm{nom}}$ are used to normalize the cost function terms. The torque reference is externally generated by a PI speed controller. The factor λ_0 denotes a weight factor.

Finally, the optimization step is carried out, and the inverter voltage vector that minimizes the cost function is selected as the optimal switching state for the next sampling period $k+1$, thus the optimal torque and flux control is achieved.

D. Time-Delay Compensation

It is well known that there is one-step delay in digital implementation. In other word, the voltage vector selected at the instant time k will not be applied until the instant time $k+1$ [33]–[35]. To eliminate this delay, the value at the instant time $k+2$ should be used in (18) rather than the instant time $k+1$.

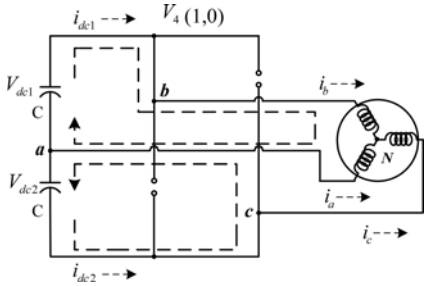

Fig. 4. Current paths in the switching state V_4.

TABLE III
MOTOR AND B4 INVERTER PARAMETERS

Parameters	Values
DC-link voltage	540 V
DC-link upper capacitor (C_1)	2040 μF
DC-link upper capacitor (C_2)	2040 μF
Dead time	4 μs
Induction motor	
Rated power	2.2 kW
Rated voltage	380 V
Rated speed	1430 r/min
Rated current	4.9 A
Rated frequency	50 Hz
Number of poles	4
Stator resistance (R_s)	2.804 Ω
Stator leakage inductance (L_s)	10.33 mH
Rotor resistance (R_r)	2.178 Ω
Rotor leakage inductance (L_r)	10.33 mH
Magnetizing inductance (L_m)	319.7 mH
Nominal flux-linkage	0.6 Wb
Rated torque	14 N·m

Therefore, the cost function (18) is redefined as

$$\boldsymbol{g}_i = \frac{\left|T_e^* - \hat{T}_e(k+2)_i\right|}{T_{e_{\text{nom}}}} + \lambda_0 \frac{\left|\left\|\vec{\Psi}_s^*\right\| - \left\|\overrightarrow{\hat{\Psi}}_s(k+2)_i\right\|\right|}{\left\|\vec{\Psi}_s\right\|_{\text{nom}}}$$
$$i \in \{1,2,3,4\}. \tag{19}$$

E. DC-Link Voltage Offset Suppression

The inappropriate initial phase angle of phase "a" current or the imbalance current flowing in the two capacitors will cause voltage deviation [15]. And as it is shown in Fig. 2, the capacitor voltage offset relates to the inverter gain increment and reliable operation of the B4 inverter. Therefore, suppressing the offset of the two capacitor voltages is necessary

Consider the switching state $V_4(1,0)$ shown in Fig. 4. Two current circuit loops are made. Applying Kirchhoff's voltage law, i_{dc1} and i_{dc2} are obtained. In the same way, the dc-link currents of the other three vectors are obtained.

The dc-link currents can also be expressed as a function of the switching states

$$i_{\text{dc1}} = i_b \cdot S_b + i_c \cdot S_c$$

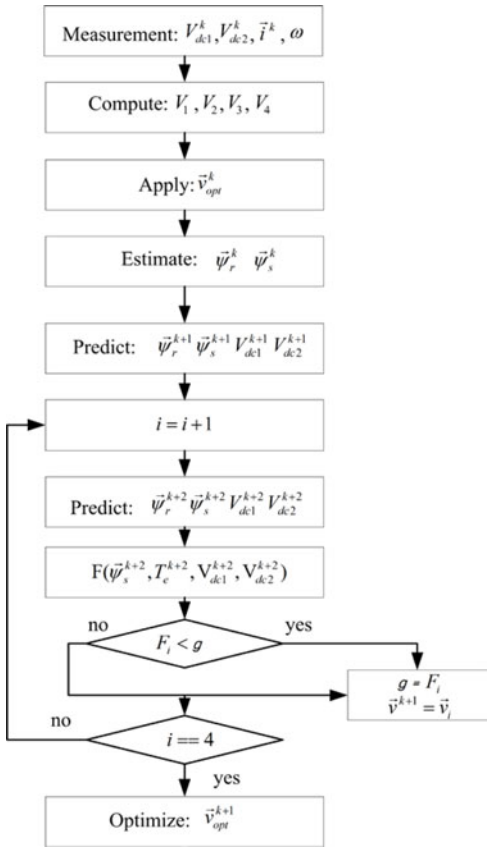

Fig. 5. Implementation flowchart of the proposed scheme.

$$i_{\text{dc2}} = i_b \cdot (1 - S_b) + i_c \cdot (1 - S_c) \tag{20}$$

where i_{dc1} and i_{dc2} are the upper and the lower dc-link currents and $\boldsymbol{i}_b$ and $\boldsymbol{i}_c$ are the phase currents. With these capacitor currents (20), the capacitor voltages are obtained

$$\hat{V}_{\text{dc1}} = V_{\text{dc1}} + (1/C)\int_{t_0}^{t}(-i_{\text{dc1}})dt$$
$$\hat{V}_{\text{dc2}} = V_{\text{dc2}} + (1/C)\int_{t_0}^{t} i_{\text{dc2}}dt \tag{21}$$

where *C* is the capacitance of the two dc-link capacitors.

Using the Euler formula to discretize (20) and shifting the result to a single time step, the capacitor currents at sample time *k* are obtained as follows:

$$i_{\text{dc1}}(k) = i_b(k) \cdot S_b + i_c(k) \cdot S_c$$
$$i_{\text{dc2}}(k) = i_b(k) \cdot (1 - S_b) + i_c(k) \cdot (1 - S_c). \tag{22}$$

Using the Euler formula to discretize (21) and shifting the result to a single time step, the predicted capacitor voltages $\hat{V}_{\text{dc1}}(k+1)$ and $\hat{V}_{\text{dc2}}(k+1)$ at time $k+1$ are obtained as follows:

$$\hat{V}_{\text{dc1}}(k+1) = \hat{V}_{\text{dc1}}(k) - (1/C) \cdot i_{\text{dc1}}(k) \cdot T_s$$
$$\hat{V}_{\text{dc2}}(k+1) = \hat{V}_{\text{dc2}}(k) + (1/C) \cdot i_{\text{dc2}}(k).T_s. \tag{23}$$

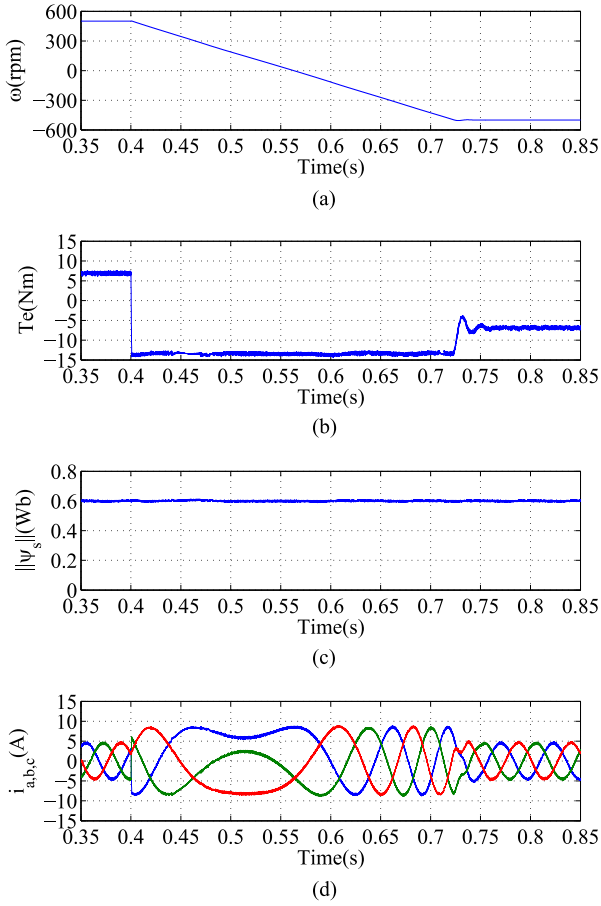

Fig. 6. Simulated waveforms using the proposed scheme in a B4 inverter-fed IM. (a) Speed, (b) developed torque, (c) stator flux, and (d) stator current behaviors during a speed-reversal maneuver at 50% rated load torque ($\lambda_0 = 3$).

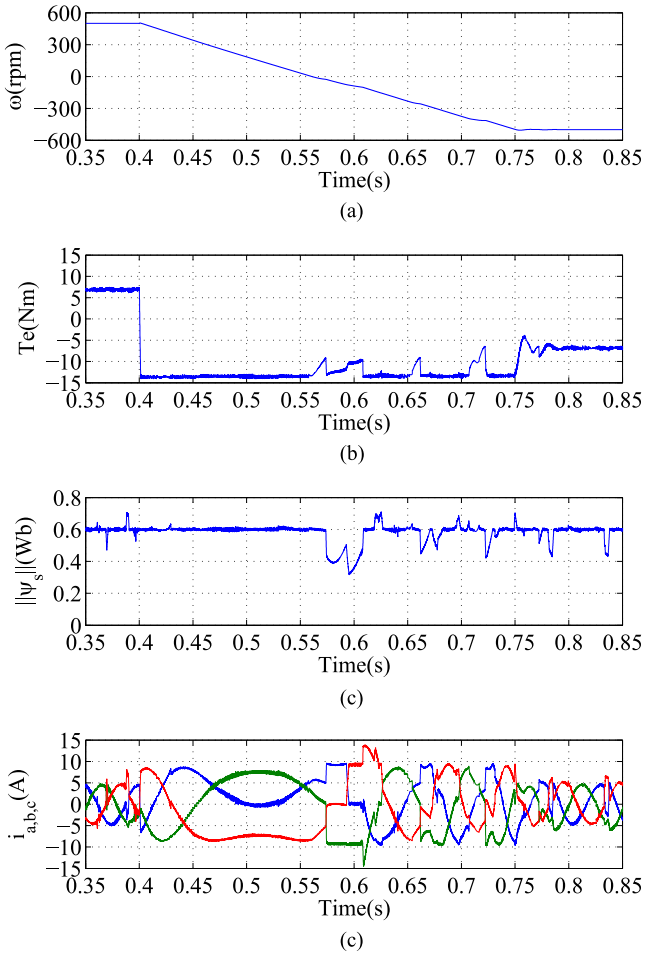

Fig. 7. Simulated waveforms using the proposed scheme in a B4 inverter-fed IM. (a) Speed, (b) developed torque, (c) stator flux, and (d) stator current behaviors during a speed-reversal maneuver at 50% rated load torque ($\lambda_0 = 1$).

The $\hat{V}_{\mathrm{dc1}}(k+2)$ and $\hat{V}_{\mathrm{dc2}}(k+2)$ can be obtained in the same way.

The cost function, including the voltage offset suppression, is given by adding a third term to the cost function (19)

$$g_i = \frac{\left|T_e^* - \hat{T}_e(k+2)_i\right|}{T_{e_{\mathrm{nom}}}} + \lambda_0 \frac{\left|\left\|\vec{\Psi}_s^*\right\| - \left\|\vec{\hat{\Psi}}_s(k+2)_i\right\|\right|}{\left\|\vec{\Psi}_s\right\|_{\mathrm{nom}}} + \lambda_{\mathrm{dc}} \frac{\left|\hat{V}_{\mathrm{dc1}}(k+2)_i - \hat{V}_{\mathrm{dc2}}(k+2)_i\right|}{V_{\mathrm{dc}}}, \quad i \in \{1,2,3,4\} \tag{24}$$

where V_{dc} is dc-link voltage, which can be obtained by $V_{\mathrm{dc}} = V_{\mathrm{dc1}} + V_{\mathrm{dc2}}$, λ_{dc} is the weight factor of the dc-link capacitor voltage offset suppression.

The minimization of (24) is done by an exhaustive search for all feasible voltage vectors. The proposed control scheme can be implemented in the following sequence (see Fig. 5). The superscript k, $k+1$, and $k+2$ denote the variables' value at sampling time k, $k+1$, and $k+2$, respectively. $\overrightarrow{v}_{\mathrm{opt}}^{k}$ and $\overrightarrow{v}_{\mathrm{opt}}^{k+1}$ are the optimal voltage vectors found in the previous loop iteration and the current loop iteration, respectively.

As it is shown earlier, a high degree of flexibility is obtained with the proposed control scheme due to the online optimization algorithm, where the system nonlinearities and restrictions (i.e., capacitor voltage offset suppression) can be included in the cost function.

IV. Analysis and Discussion on Weighting Factors

In the proposed scheme, as it is clear in (24) that the only parameters to adjust are the weighting factors in the cost function. Therefore, it is necessary to analyze and discuss the effects of these parameters. However, there is no formal method to obtain the optimum value of these parameters to the date. Hence, these values are obtained by a simulation-based heuristic procedure. In order to analyze the effects of weighting factors, extensive simulations are performed in MATLAB/Simulink. This environment allows comparing the performance of different weighting factors. The ratings and parameters of the B4 inverter and induction machine, used in the simulation as well

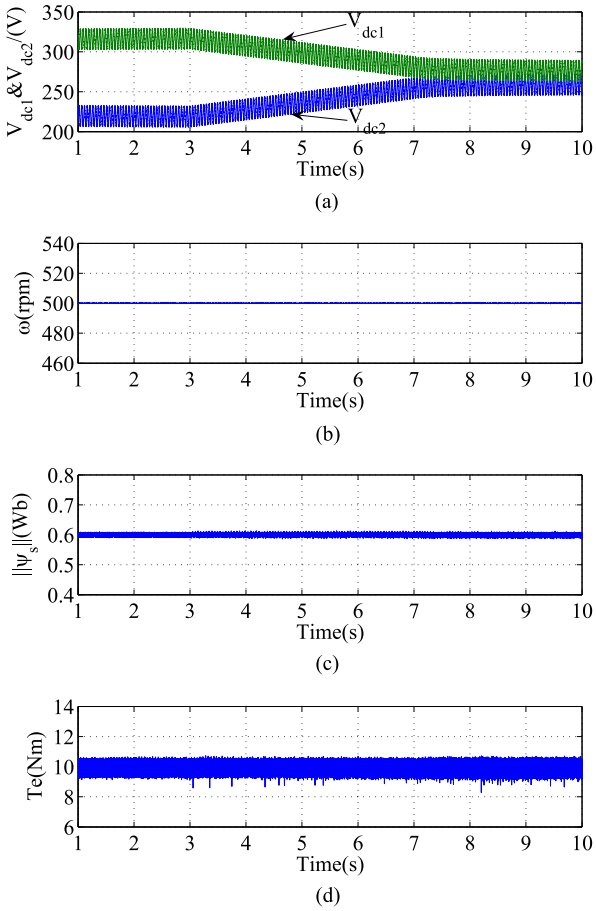

Fig. 8. Simulated two capacitor voltages with offset suppression method. (a) Capacitor voltages, (b) speed, (c) stator flux, and (d) developed torque behaviors during a voltage suppression method applied ($\lambda_{\rm dc} = 1000$).

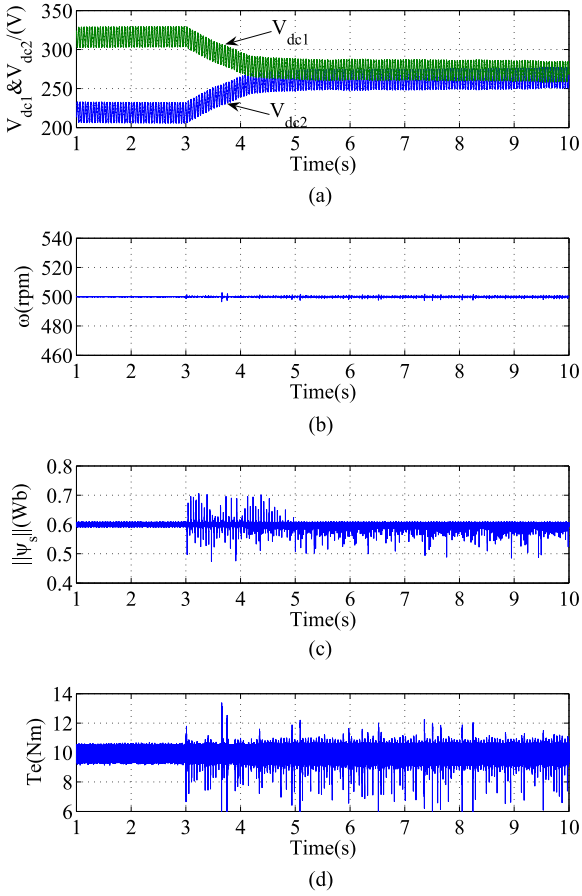

Fig. 9. Simulated two capacitor voltages with offset suppression method. (a) Capacitor voltages, (b) speed, (c) stator flux, and (d) developed torque behaviors during a voltage suppression method applied ($\lambda_{\rm dc} = 2000$).

as in the experimental study, are listed in Table III. The details are analyzed and discussed later.

A. Stator Flux Weighting Factor λ_0

λ_0 is a weighting factor that increases or decreases the relative importance of the torque versus flux control. If the same importance is assigned to both control objectives, this factor is given as $\lambda_0 = 1$. Since the currents are forced by directly controlling the stator flux, to obtain the balanced currents versus the unbalanced structure of B4 inverter, a higher weighting factor λ_0 is expected (e.g., $\lambda_0 = 3$).

Fig. 6 presents the simulation results using the proposed scheme in a B4 inverter-fed IM during a speed-reversal maneuver from 500 to –500 r/min at 50% rated load torque for the case of $\lambda_0 = 3$, where the stator flux reference is the nominal one at 0.6 Wb. A comparable study for the same system but considering a smaller weighting factor, namely, $\lambda_0 = 1$ are presented in Fig. 7. Here, it can be appreciated that the flux exhibits a higher ripple during steady state when compared to the previous case. Additionally, it can be noticed that, during the transient, the balanced three-phase currents collapse due to the failure in stator flux control. Henceforth, considering the good performance obtained, in the remaining tests, the tuning factors λ_0 will be kept at the value of $\lambda_0 = 3$.

B. Capacitor Voltages Offset Suppression Weighting Factor

The weighting factor $\lambda_{\rm dc}$ denotes a weight factor, which increases or decreases the relative importance of the dc-link capacitor voltage offset suppression versus the control performance. With a higher value of the weighting factor $\lambda_{\rm dc}$, the two capacitor voltages converge faster, but when a very high value of this weighting factor is applied, the control performance is affected.

In order to analyze the effects of weighting factors $\lambda_{\rm dc}$, the simulation results at the speed of 500 r/min with a torque of $10\ {\rm N}\cdot{\rm m}$ are shown in Figs. 8 and 9 in case of $\lambda_{\rm dc} = 1000$ and $\lambda_{\rm dc} = 2000$, respectively. The capacitor voltage, electromagnetic torque, stator flux, and speed waveform behaviors during the voltage suppression method added are shown. The voltage offset is obvious before the suppression method applied. In Fig. 8, after the voltage offset suppression term is added at $t = 3$ s, the two capacitor voltages converge to 270 V at $t = 7$ s, and as it is shown that a slight increment in the torque ripple occurs when the capacitor voltage offset term is added. This is acceptable with negligible effect on the flux and speed waveforms. For a comparative study, the results in the cases of $\lambda_{\rm dc} = 2000$ are carried out in Fig. 9. It can be noticed that the

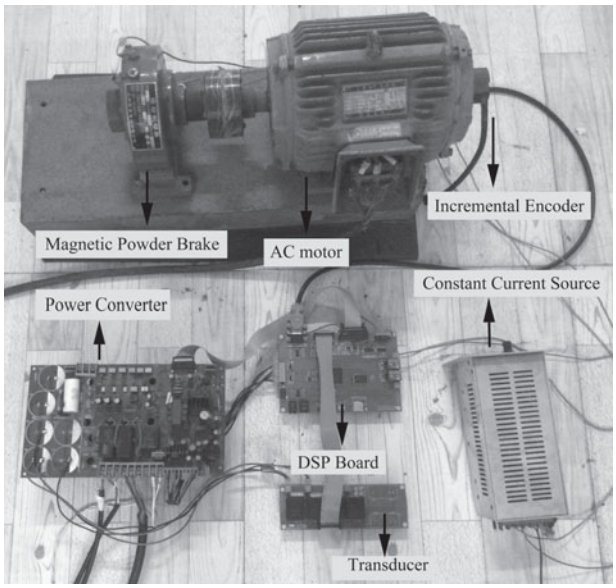

Fig. 10. Experimental setup.

converging time of the two capacitor voltages is approximately 1 s, but a significant stator flux and torque ripples are exhibited in the steady state. The aforementioned effect of $\lambda_{\rm dc}$ is validated. In consideration of the good performance obtained, in the remaining tests, the tuning factors $\lambda_{\rm dc}$ will be kept at the value of $\lambda_{\rm dc} = 1000$.

V. Experimental Results

The experimental setup, as shown in Fig. 10, incorporates a control board, which is based on the 32-bit floating point DSP TI TMS320F28335. Two phase currents i_a and i_b and two capacitor voltages $V_{\rm dc1}$ and $V_{\rm dc2}$ are sensed by the Hall-effect current and voltage sensors, respectively. These currents and voltages are fed to the DSP through the signal processing circuit. Furthermore, the position of the rotor is sensed by an incremental encoder and fed to the encoder interface on the DSP board. The generated pulses are then transmitted to the gate drives of the IGBTs (PM25RSB120). The sampling time for experimental implementation is determined to be 40 μs. Regarding to the proposed PTC computational effort, the tested calculation time is 13.4 μs. The speed control loop is implemented at a subsampled rated of 1000 Hz in order to reduce the quantization error in the speed signal derived from the incremental encoder. All the experimental data was saved to the DSP RAM every two sampling period, namely, 80 μs, and it was read by an emulator that was connected to the computer. The magnetic powder brake driven by a constant current source is used as load. However, it is not an ideal step changed load, which causes a little mismatch of the simulation and experimental results.

The dynamic behaviors of the speed, electromagnetic torque, stator flux, and stator current during from 500 to –500 r/min at 30% of the rated load torque are presented in Fig. 11. The speed reversal command is applied at 0.16 s. The balanced three-phase currents are obtained. A quick transient speed response with max

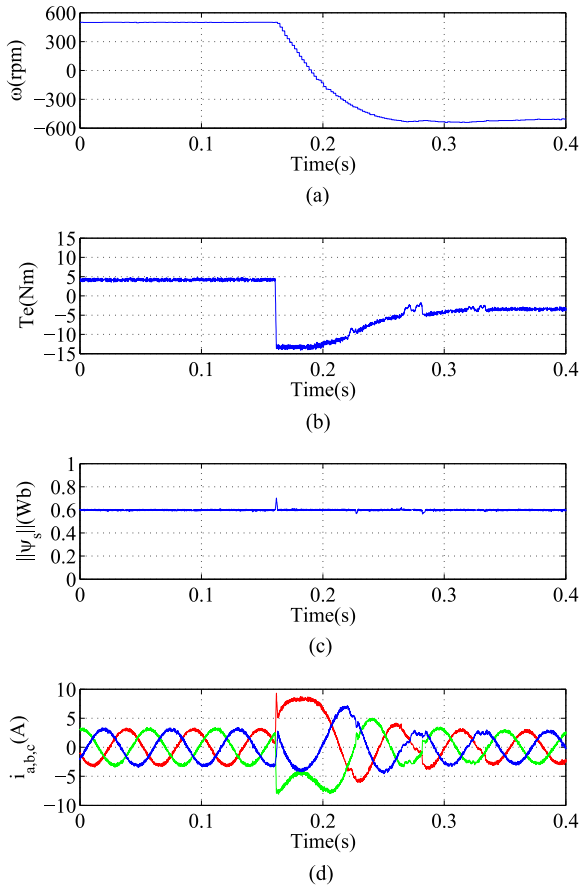

Fig. 11. Experimental waveforms using the proposed scheme in a B4 inverter-fed IM. (a) Speed, (b) developed torque, (c) stator flux, and (d) stator current behaviors during a speed-reversal maneuver at 50% rated load torque.

torque reverse demonstrates the high dynamic performances of the proposed scheme.

Fig. 12 shows the speed, torque, stator flux, and current dynamics of the load change from 0 to 5 $\rm N \cdot m$ with a speed of 500 r/min at 0.16 s. The load change is removed at 0.95 s. It can be observed that, the dynamic and steady speed control performance under load disturbance is acceptable.

Experimental results for the capacitor voltage offset suppression are shown in Fig. 13. With the suppression method applied at $t = 2$ s, the two capacitor voltages converge. It is shown that the capacitor voltage offset term has no effect on the torque, flux, and speed waveforms. The experimental results that are consistent with the simulation results validate the effectiveness of the proposed scheme.

Steady-state experimental results of the stator flux locus described in the $\alpha\beta$ plane with 30% rated load torque at a speed of 500 r/min are presented in Fig. 14. It is clear that the stator flux produces good waveforms. As a consequence, the balanced three-phase currents are obtained in steady state. The fast Fourier transform (FFT) results are carried out for this analysis. As shown in Table IV, there are nearly no difference in the amplitudes and the total harmonic distortion (THD) among the three-phase currents.

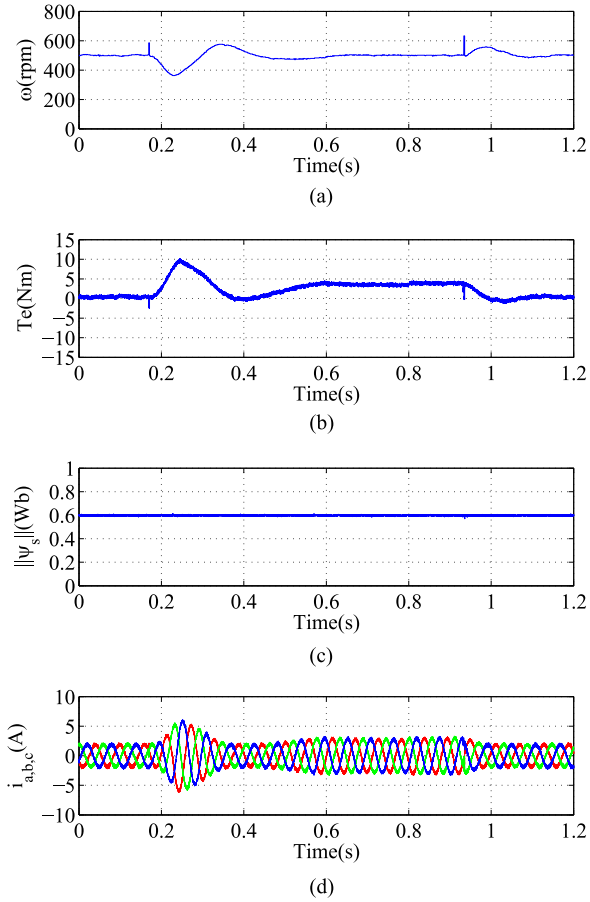

Fig. 12. Experimental results for the change in load at a speed of 500 r/min. (a) Speed, (b) developed torque, (c) stator flux, and (d) stator current behaviors during the load change.

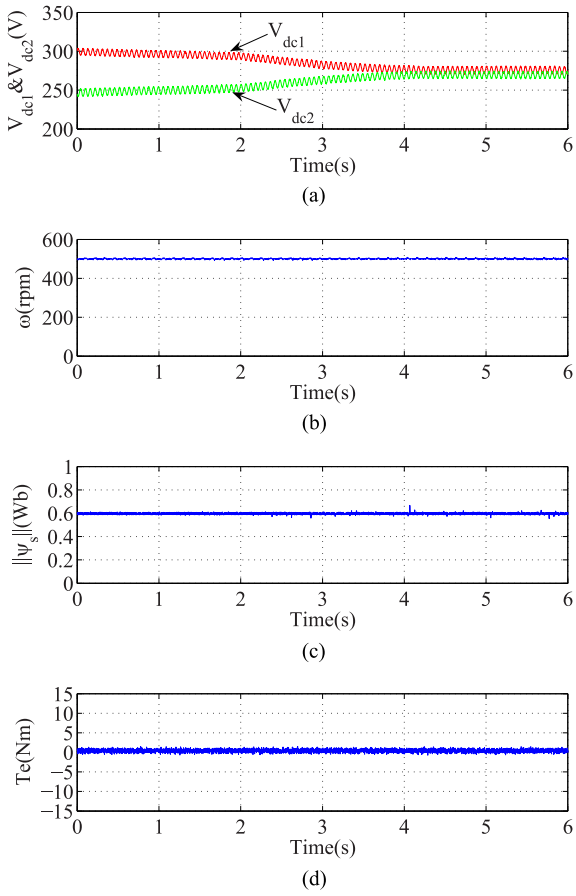

Fig. 13. Experimental results of two capacitor voltages with offset suppression method. (a) Capacitor voltages, (b) speed, (c) stator flux, and (d) developed torque behaviors during a voltage suppression method applied.

TABLE IV
THD AND RMS VALUES OF THE STATOR CURRENTS

Phase Currents	i_a	i_b	i_c
THD (%)	4.05	3.71	3.92
RMS (A)	2.83	2.84	2.86

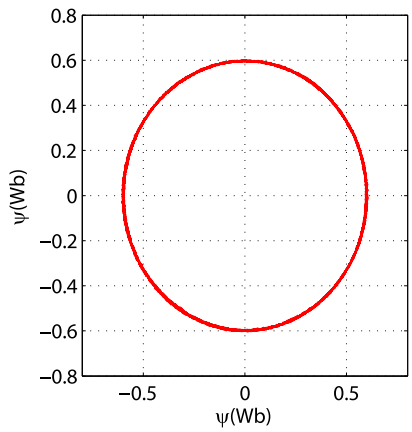

Fig. 14. Steady-state experimental result of stator flux locus described in the $\alpha\beta$ plane.

VI. CONCLUSION

In this paper, the special issues on using the famous PTC control scheme for a B4 inverter-fed IM drives are analyzed and discussed. The voltage vectors of the B4 inverter under the fluctuation of the two dc-link capacitor voltages are derived for precise prediction and control of the torque and stator flux. The balanced three-phase currents are achieved and the capacitor voltage offset is suppressed in the proposed scheme. The theory, design, and performance evaluation of the proposed scheme for the B4 inverter-fed IM drive are investigated. The proposed B4 inverter-fed IM drive has been found acceptable for high performance industrial variable-speed-drive applications considering its cost reduction and other inherent advantageous features. Certainly, the additional work is still remained to develop more efficient PTC scheme and answers the remaining questions: the robustness toward parameter deviation, parameter sensitivity of this scheme, for the parameter values may vary in the motor drives, while in other cases it is difficult to get a precise value of the parameters.

REFERENCES

[1] H. W. Van der Broeck and J. D. Van Wyk, "A comparative investigation of a three-phase induction machine drive with a component minimized voltage-fed inverter under different control options," *IEEE Trans. Ind. Appl.*, vol. IA-20, no. 2, pp. 309–320, Mar. 1984.

[2] B. A. Welchko, T. A. Lipo, T. M. Jahns, and S. E. Schulz, "Fault tolerant three-phase AC motor drive topologies: A comparison of features, cost, and limitations," *IEEE Trans. Power Electron.*, vol. 19, no. 4, pp. 1108–1116, Jul. 2004.
[3] R. L. D. Ribeiro, C. B. Jacobina, E. R. C. da Silva, and A. M. N. Lima, "Fault-tolerant voltage-fed PWM inverter AC motor drive systems," *IEEE Trans. Ind. Electron.*, vol. 51, no. 2, pp. 439–446, Apr. 2004.
[4] D. Campos-Delgado, D. Espinoza-Trejo, and E. Palacios, "Fault-tolerant control in variable speed drives: A survey," *Electric Power Appl., IET*, vol. 2, no. 2, pp. 121–134, 2008.
[5] F. Jen-Ren and T. A. Lipo, "A strategy to isolate the switching device fault of a current regulated motor drive," in *Proc. IEEE Ind. Appl. Soc. Annu. Meeting, Conf. Rec.*, 1993, vol. 2, pp. 1015–1020.
[6] T. Elch-Heb and J. P. Hautier, "Remedial strategy for inverter-induction machine system faults using two-phase operation," in *Proc. 5th Eur. Conf. Power Electron. Appl.*, 1993, vol. 5, pp. 151–156.
[7] P. N. Enjeti and A. Rahman, "A new single-phase to three-phase converter with active input current shaping for low cost AC motor drives," *IEEE Trans. Ind. Appl.*, vol. 29, no. 4, pp. 806–813, Jul./Aug. 1993.
[8] A. M. S. Mendes, X. M. Lopez-Fernandez, and A. J. M. Cardoso, "Thermal performance of a three-phase induction motor under fault tolerant operating strategies," *IEEE Trans. Power Electron.*, vol. 23, no. 3, pp. 1537–1544, May 2008.
[9] D. Sun, Z. Y. He, Y. K. He, and Y. F. Guan, "Four-switch inverter fed PMSM DTC with SVM approach for fault tolerant operation," in *Proc. IEEE Int. Electric Machines Drives Conf.*, 2007, vol. 1–2, pp. 295–299.
[10] L. Tian-Hua, F. Jen-Ren, and T. A. Lipo, "A strategy for improving reliability of field-oriented controlled induction motor drives," *IEEE Trans. Ind. Appl.*, vol. 29, no. 5, pp. 910–918, Sep./Oct. 1993.
[11] M. B. D. Correa, C. B. Jacobina, E. R. C. da Silva, and A. M. N. Lima, "A general PWM strategy for four-switch three-phase inverters," *IEEE Trans. Power Electron.*, vol. 21, no. 6, pp. 1618–1627, Nov. 2006.
[12] F. Blaabjerg, D. O. Neacsu, and J. K. Pedersen, "Adaptive SVM to compensate DC-Link voltage ripple for four-switch three-phase voltage-source inverters," *IEEE Trans. Power Electron.*, vol. 14, no. 4, pp. 743–752, Jul. 1999.
[13] J. Kim, J. Hong, and K. Nam, "A current distortion compensation scheme for four-switch inverters," *IEEE Trans. Power Electron.*, vol. 24, no. 3–4, pp. 1032–1040, Mar.–Apr. 2009.
[14] D. M. Lee, J. B. Park, and H. A. Toliyat, "A simple current ripple reduction method for B4 inverters," *J. Elect. Eng. Technol.*, vol. 8, no. 5, pp. 1062–1069, Sep. 2013.
[15] R. Wang, J. Zhao, and Y. Liu, "A comprehensive investigation of four-switch three-phase voltage source inverter based on double Fourier integral analysis," *IEEE Trans. Power Electron.*, vol. 26, no. 10, pp. 2774–2787, Oct. 2011.
[16] M. N. Uddin, T. S. Radwan, and M. A. Rahman, "Fuzzy-logic-controller-based cost-effective four-switch three-phase inverter-fed IPM synchronous motor drive system," *IEEE Trans. Ind. Appl.*, vol. 42, no. 1, pp. 21–30, Jan.–Feb. 2006.
[17] S. A. R. Kashif, M. A. Saqib, and S. Zia, "Implementing the induction-motor drive with four-switch inverter: An application of neural networks," *Expert Syst. Appl.*, vol. 38, no. 9, pp. 11137–11148, Sep. 2011.
[18] B. El Badsi, B. Bouzidi, and A. Masmoudi, "DTC scheme for a four-switch inverter-fed induction motor emulating the six-switch inverter operation," *IEEE Trans. Power Electron.*, vol. 28, no. 7, pp. 3528–3538, Jul. 2013.
[19] J. H. Lee, "Model predictive control: Review of the three decades of development," *Int J Control Autom.*, vol. 9, no. 3, pp. 415–424, Jun. 2011.
[20] J. Holtz and S. Stadtfeldt, "A predictive controller for the stator current vector of ac machines fed from a switched voltage source," in *Proc. IEEE IPEC*, 1983, vol. 2, pp. 1665–1675.
[21] R. Kennel and D. Schöder, "A predictive control strategy for converters," in *Proc. IFAC Control Power Electron. Elect. Drives*, 1983, pp. 415–422.
[22] A. Linder, R. Kanchan, R. Kennel, and P. Stolze, *Model-Based Predictive Control of Electric Drives*, Munich, Germany: Cuvillier Verlag Göttingen, 2010.
[23] S. Mariethoz, M. Herceg, and M. Kvasnica, "Model predictive control of buck DC-DC converter with nonlinear inductor," in *Proc. 11th Workshop Control Model. Power Electron.*, 2008, pp. 1–8.
[24] P. Cortes, J. Rodriguez, P. Antoniewicz, and M. Kazmierkowski, "Direct power control of an AFE using predictive control," *IEEE Trans. Power Electron.*, vol. 23, no. 5, pp. 2516–2523, Sep. 2008.
[25] S. Mariethoz, A. Domahidi, and M. Morari, "Sensorless explicit model predictive control of permanent magnet synchronous motors," in *Proc. IEEE Electric Machines Drives Conf., Int.*, 2009, pp. 1250–1257.
[26] T. Geyer, G. Papafotiou, and M. Morari, "Model predictive direct torque control—Part I: Concept, algorithm, and analysis," *IEEE Trans. Ind. Electron.*, vol. 56, no. 6, pp. 1894–1905, Jun. 2009.
[27] G. Papafotiou, J. Kley, K. G. Papadopoulos, P. Bohren, and M. Morari, "Model predictive direct torque control–Part II: Implementation and experimental evaluation," *IEEE Trans. Ind. Electron.*, vol. 56, no. 6, pp. 1906–1915, Jun. 2009.
[28] S. Kouro, P. Cortés, R. Vargas, U. Ammann, and J. Rodríguez, "Model predictive control—A simple and powerful method to control power converters," *IEEE Trans. Ind. Electron.*, vol. 56, no. 6, pp. 1826–1838, 2009.
[29] C. A. Rojas, J. Rodriguez, F. Villarroel, J. R. Espinoza, C. A. Silva, and M. Trincado, "Predictive torque and flux control without weighting factors," *IEEE Trans. Ind. Electron.*, vol. 60, no. 2, pp. 681–690, Feb. 2013.
[30] P. Cortes, M. P. Kazmierkowski, R. M. Kennel, D. E. Quevedo, and J. Rodriguez, "Predictive control in power electronics and drives," *IEEE Trans. Ind. Electron.*, vol. 55, no. 12, pp. 4312–4324, Dec. 2008.
[31] H. Miranda, P. Cortes, J. I. Yuz, and J. Rodriguez, "Predictive torque control of induction machines based on state-space models," *IEEE Trans. Ind. Electron.*, vol. 56, no. 6, pp. 1916–1924, Jun. 2009.
[32] J. Rodriguez, J. Pontt, C. A. Silva, P. Correa, P. Lezana, P. Cortes, and U. Ammann, "Predictive current control of a voltage source inverter," *IEEE Trans. Ind. Electron.*, vol. 54, no. 1, pp. 495–503, Feb. 2007.
[33] J. Rodriguez, R. M. Kennel, J. R. Espinoza, M. Trincado, C. A. Silva, and C. A. Rojas, "High-performance control strategies for electrical drives: An experimental assessment," *IEEE Trans. Ind. Electron.*, vol. 59, no. 2, pp. 812–820, Feb. 2012.
[34] P. Cortes, J. Rodriguez, C. Silva, and A. Flores, "Delay compensation in model predictive current control of a three-phase inverter," *IEEE Trans. Ind. Electron*, vol. 59, no. 2, pp. 1323–1325, Feb. 2012.
[35] Y. Zhang, J. Zhu, and W. Xu, "Analysis of one step delay in direct torque control of permanent magnet synchronous motor and its remedies," in *Proc. Int. Conf. Elect. Machines Syst.*, 2010, pp. 792–797.
[36] M. Habibullah and D. D. C. Lu, "Predictive torque and flux control of a four-switch inverter-fed IM drive," in *Proc. 1st Int. Future Energy Electron. Conf.*, 2013, pp. 629–634.

Dehong Zhou was born in Sichuan Province, China, in 1989. He received the B.S. degree from the Department of Control Science and Engineering, Huazhong University of Science and Technology (HUST), Wuhan, China, in 2012. He is currently working toward the Ph.D. degree at the School of Automation, HUST.

His research interests include power electronics, high performance AC motor drives, predictive control and fault tolerant control.

Jin Zhao (M'14) was born in Hubei Province, China, in 1967. He received the B.E. and Ph.D. degrees from the Department of Control Science and Engineering, Huazhong University of Science and Technology (HUST), Wuhan, China, in 1989 and 1994, respectively.

Since 2004, he has been a Full Professor with the School of Automation, HUST. During 2001–2002, he was a Visiting Scholar in the Power Electronics Research Laboratory, University of Tennessee, Knoxville, USA. He is currently involved in research and applications of power electronics, electrical drives, fault diagnosis, and intelligent control. He is the author or coauthor of more than 100 technical papers.

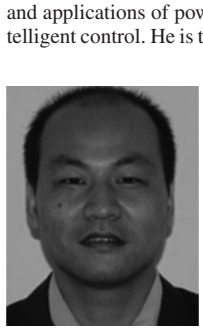

Yang Liu (M'12) was born in Hubei Province, China, in 1979. He received the B.E. degree in automation from Wuxi Light Industry University (now Jiangnan University), Wuxi, China, in 2000, the M.E. and the Ph.D. degrees in control science and engineering from the Department of Control Science and Engineering, Automation Institute, Huazhong University of Science and Technology (HUST), Wuhan, China, in 2005 and 2009, respectively.

He is currently a Lecturer at the School of Automation, HUST. His current research interests include power electronics, high-performance ac motor drives, and fault diagnosis.